AECL-10312

ATOMIC ENERGY OF CANADA LIMITED

ÉNERGIE ATOMIQUE DU CANADA LIMITÉE

RF FIELD CONTROL FOR KAON FACTORY BOOSTER CAVITIES

RÉGLAGE DU CHAMP RF DES CAVITÉS D'AMPLIFICATION D'UNE USINE DE KAONS

S.T. CRAIG and M.S. de JONG

Chalk River Laboratories

Laboratoires de Chalk River

Chalk River, Ontario K0J 1J0

November 1990 novembre

AECL Research

RF Field Control for Kaon Factory Booster Cavities

S.T. Craig and M.S. de Jong

Accelerator Physics Branch
Chalk River Laboratories
Chalk River, Ontario, Canada K0J 1J0

1990 November

AECL-10312

EACL Recherche

RÉGLAGE DU CHAMP RF DES CAVITÉS D'AMPLIFICATION D'UNE USINE DE KAONS

S.T. Craig et M.S. de Jong

RÉSUMÉ

On procède actuellement à l'étude de conception d'un système de réglage les champs d'accélération RF de l'accélérateur intermédiaire de l'usine de kaons. Ce concept porte sur le réglage de la cavité résonnante: réglage, amplitude de tension et phase de tension. On a élaboré des simulations avec plage de temporisation afin d'évaluer les dispositifs de réglage proposés. Ces simulations indiquent qu'il est possible d'obtenir un réglage de fréquence acceptable grâce à une combinaison de précompensation adaptative et de réglage de réaction rigide. L'amplitude de tension et la phase de tension peuvent être réglées de façon adéquate par précompensation non adaptative en combinaison avec un réglage de réaction rigide.

Ces travaux ont été effectués en sous-traitance par TRIUMF, à Vancouver, en Colombie-Britannique, Canada

Division de la Physique des accélérateurs
Laboratoires de Chalk River
Chalk River (Ontario), Canada K0J 1J0

Novembre 1990

AECL-10312

AECL Research

RF Field Control for Kaon Factory Booster Cavities

S.T. Craig and M.S. de Jong

ABSTRACT

A conceptual design is developed for control of the Kaon Factory Booster rf accelerating fields. This design addresses control of cavity: tuning, voltage amplitude, and voltage phase angle. Time-domain simulations were developed to evaluate the proposed controllers. These simulations indicate that adequate tuning performance can be obtained with the combination of adaptive feedforward and proportional feedback control. Voltage amplitude and voltage phase can be adequately controlled using non-adaptive feedforward and proportional feedback control.

This work was performed under contract to TRIUMF, Vancouver, B.C., Canada

Accelerator Physics Branch
Chalk River Laboratories
Chalk River, Ontario, Canada K0J 1J0

1990 November

AECL-10312

CONTENTS

1.0 INTRODUCTION

The proposed Kaon Factory will consist of the present TRIUMF cyclotron, for injection, and five synchrotrons: the Accumulator, Booster, Collector, Driver, and Extender (A,B,C,D, and E rings, respectively) [1]. Proton acceleration is done in the Booster and Driver. The Booster increases proton energy from 500 MeV to 3 GeV; the Driver completes the acceleration to 30 GeV. Compared to the Driver, the Booster must operate over a wide frequency range, because of the wide energy range and comparatively low injection energy. The 46.11 MHz to 60.75 MHz Booster operation presents significant control challenges in the areas of resonant cavity tuning and accelerating field control. Control is further challenged by the fast 10 ms ramp over this operating range.

The conceptual design calls for ferrite tuning of the cavity resonant frequency and wideband feedback control of the accelerating voltage [2]. Controller design and performance for these two aspects is the topic of this report. The scope of this work is limited to the local control of a single cavity's resonant frequency and voltage. It is assumed that an accurate rf reference signal is provided.

The work proceeded as follows:

- The control problem was examined using a first-order analytical and simulation-based approach. Various control options were evaluated.
- The most promising controller design was selected and evaluated using a detailed simulation.
- An outline was developed for the hardware required to implement the controller.

Two entirely separate simulations were developed: one to examine tuning control, the other to evaluate direct fast-feedback with feedforward. Separate simulations were used due to the difference in time scales between the tuning and cavity-field controllers. Further, it is assumed that the two controllers are not cross-coupled. Both simulations are written in Fortran and use the IMSL fifth-order variable step-size Runge-Kutta integration algorithm [3].

An explanation of the operating specifications as they pertain to the control problem is given. Results of the three work stages listed above are then reported.

2.0 PROBLEM DESCRIPTION

2.1 Notation

Throughout this report, the notation used is as shown in the phasor diagram below:

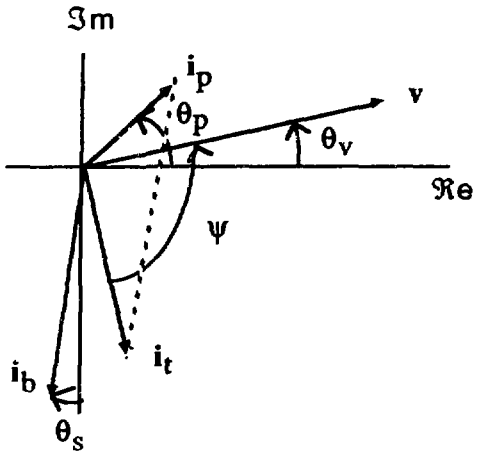

Figure 2-1: Phasor Diagram

where:

i_p	final amplifier plate current	i_b	beam current
i_t	total of i_p and i_b	v	cavity gap voltage
θ_s	synchronous phase angle	ψ	detuning angle
Y	$\lvert i_b \rvert \div \lvert i_p \rvert$ = beam loading factor	j	$\sqrt{-1}$

Other notation:

ω_0, f_0	resonant frequency in radians/s, Hz	$\Delta\omega$, Δf	deviation from resonance
Q	quality factor	s	Laplace variable
Q_L	loaded Q	i_s	tuner solenoid current

Symbolism used in block diagrams:


summing junction


splitter/combiner


mixer, multiplier


hybrid junction

lowpass filter

bandpass filter


amplifier

power supply


phase shifter

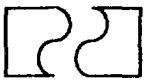
delay line


current source


variable attenuator

2.2 Scope

The scope of this study comprises design of a local controller for cavity tuning and rf voltage regulation. The term "local" refers to controllers that regulate a cavity's accelerating voltage relative to a setpoint. The setpoint is derived by non-local control loops, which regulate such variables as beam radial position, and phase. While local controllers manipulate sub-systems, such as the rf amplifier chain, the design of these sub-systems is considered to be fixed and beyond the scope of this design work.

A block diagram of the local controllers is given in Figure 2-2. Control is divided into two areas: cavity voltage and cavity tuning (resonance control). Controller designs that were considered, and their operation, are summarized in Table 2-1.

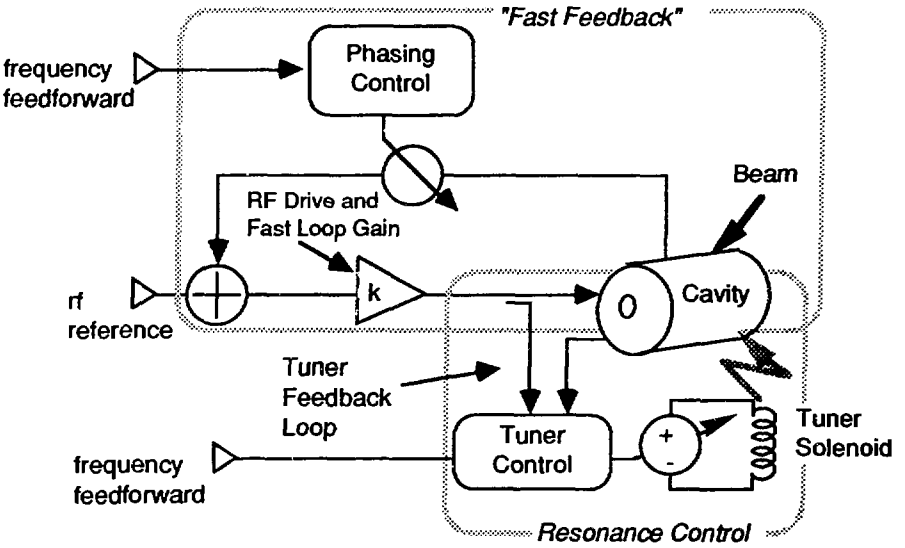

Figure 2-2: Cavity - rf Control Loops

Table 2-1: Controller Options Considered

Controller	Basic Operation
tuning feedback	The phase angle of the cavity rf field relative to the rf drive is used to indicate tuning error. This error signal is amplified and used as the control input to the tuning solenoid power supply, which in turn adjusts cavity resonance.
tuning feedforward	Advance knowledge of the drive frequency is used to set the tuner solenoid current, based on measured system dynamics.
direct fast-feedback	A low-power sample of the cavity rf field is compared with a rf reference signal. The difference between these signals is amplified and used to drive the cavity.
feedback phasing	For direct fast-feedback to be stable, the transit time around the loop must be such that the cavity signal will be subtracted from the reference. This requires an effective loop length of $n\lambda/2$. The feedback phasing controller uses advance knowledge of the drive frequency to adjust the feedback loop phase.
baseband fast-feedback	The need for feedback phasing is avoided if the cavity feedback signal is coherently down-converted into in-phase and quadrature baseband signals. These signals are compared to in-phase and quadrature setpoints and the difference is amplified, as in the direct fast-loop. The amplified error signal is coherently up-converted prior to input to the drive chain.
rf feedforward	The time of beam injection and the timing of empty buckets can be measured along with beam magnitude. This information is used to synchronously correct the rf drive based on the expected response of the drive chain and cavity.

2.3 Operating Conditions

Operating parameters relevant to control of the Booster cavities are taken from [2] and repeated below:

frequency:	46.11 to 60.75 MHz
harmonic number:	45
loaded Q:	3000 to 5000
R/Q:	35
Gap Voltage, V:	30.4 to 62.5 kV/cavity (12 cavities)
Max. amplifier dissipation:	150 kW
Max. loop delay:	70 ns (fast feedback)
Charge of beam:	1.92 μC
Bucket filling:	40 of 45 buckets, injection/ejection is done within one revolution interval
Tuner R,L:	2 mΩ, 400 μH
Tuner power supply:	20% excess capacity, 0.125% tracking during nominal 10 ms ramp.
Acceleration Cycle:	10 ms acceleration, 10 ms recovery

The voltage, synchronous phase and frequency as a function of time are given for the acceleration cycle in Figure 2-3. In Figure 2-4, cavity resonance is shown as a function of tuner solenoid current.

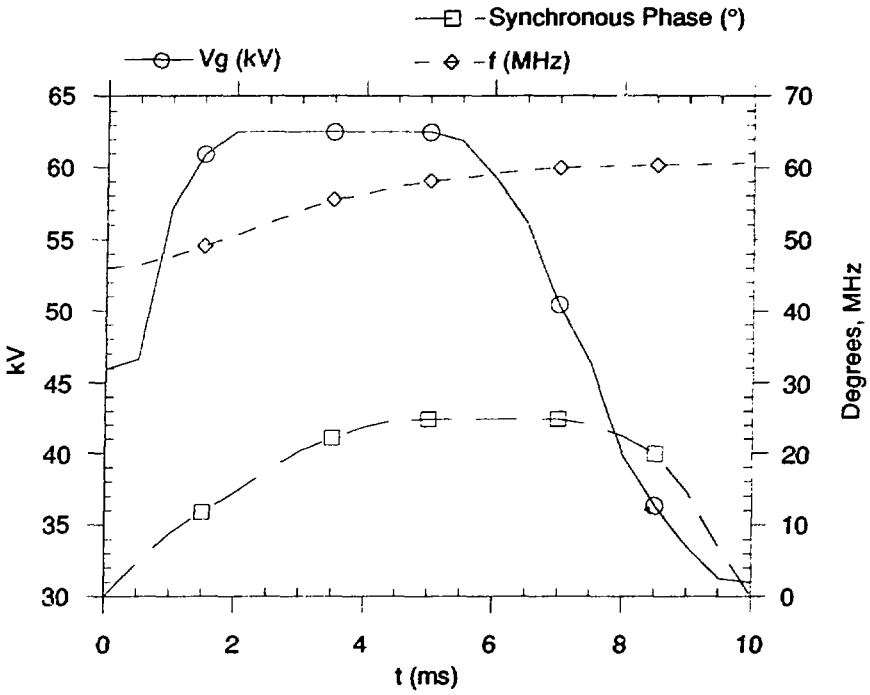

Figure 2-3: Booster Acceleration Cycle

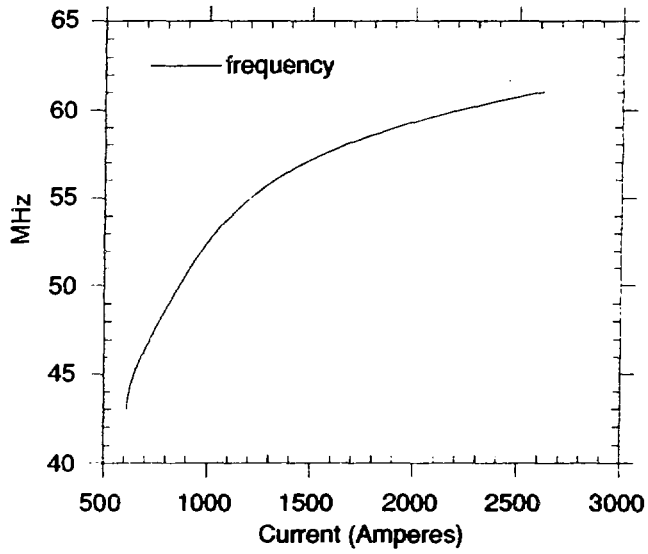

Figure 2-4: Cavity Resonance Versus Tuner Current [4]

2.4 Performance Goals

Specifications for accelerating voltage and phase regulation were not available at the time of this study. However, tolerances for uncorrelated noise are given as: $|\Delta v|/|v| \leq 0.3\%$ rms and $|\Delta\theta_v| < 2.3°$ rms [5]. Therefore, 0.3% rms amplitude and 2.3° rms phase are used as criteria for deviations in **v**. When a fast-feedback loop regulates **v**, the primary impact of tuning accuracy is on electrical efficiency. Arbitrarily setting a tolerance of 5% inefficiency due to tuning error translates into a ±12° regulation requirement on Ψ. Using a cavity Q_L of 4000, ±12° corresponds to ±1.2 kHz for f_0= 46 MHz and ±1.6 kHz at f_0 = 61 MHz.

Regulation is to be maintained under the conditions listed in §2.3.

3.0 LOOP INTERACTIONS

Two cavity-rf control loops will be used to maintain the cavity gap voltage in agreement with an rf reference. A tuning control loop compensates the average beam loading and reduces the power demand. The fast feedback loop provides compensation for beam transients. The arrangement of these loops is sketched in Figure 2-2. Two aspects are specific to the wide range, fast, frequency swing: the feedback phasing control, and the use of frequency feedforward for both the tuner and the feedback phasing. The interaction between these loops and with other loops is identified prior to examining loop feasibility because these interactions may impose additional constraints.

Feedback phasing is required to maintain adequate phase margin over the 15 MHz frequency swing. As explained in §5.1.2, feedback phasing errors affect the amplitude and phase of **v** relative to the rf reference. Phase error in **v** couples directly to control of the synchronous phase, θ_S. Coupling of feedback phasing to fast-feedback stability can be avoided using the baseband fast-feedback, as explained in §5.1.3.

Tuning control actions are also coupled to the amplitude and phase of **v**, although this coupling is reduced by a factor equal to the open-loop gain of the fast feedback. More significantly, resonance controller performance influences the power demand on the power amplifiers and fast-feedback phasing. Coupling of the fast feedback to the resonance control is avoided by use of an amplitude insensitive phase detector, as covered in §4.1.

In the final design, baseband feedback is selected for the fast-loop; consequently, interaction with a feedback phasing controller is not an issue. In addition to the use of an amplitude-insensitive tuning error measurement, the closed loop tuning response is at least 100 times slower than the fast-loop. Therefore, the tuner control and fast-loop can be treated separately.

4.0 TUNER

4.1 Initial Evaluation

The challenge of Booster resonance control is to force accurate control on the time scale of tens of micro-seconds, from a tuning coil that has a time constant of 200 ms. The feasibility of this endeavour is considered by examining the response of the loop with a nominal controller. Both ramp and step responses are examined to predict loop performance during beam arrival/departure, and during frequency ramps.

A block diagram of the resonance feedback loop is given in Figure 4-1. This loop operates on the phase difference between the rf drive into the cavity, $\mathbf{i}_p$, and the field generated in the cavity, **v**. An automatic level control (ALC) circuit, normalizes the phase difference over the operating range of

|v|. Because of the single sensor, dual channel configuration, the ALC also adjusts the level of the rf-drive mixer-input such that the mixer output is proportional to the tuning frequency error, not the phase error (see Appendix A). Consequently, the simplified model of Figure 4-2 may be used for first-order analysis, with the further assumption that the ALC bandwidth is much greater than the overall resonance loop bandwidth. An alternative design for measuring frequency error is to use a vector demodulator and divider, as shown in Figure 4-3.

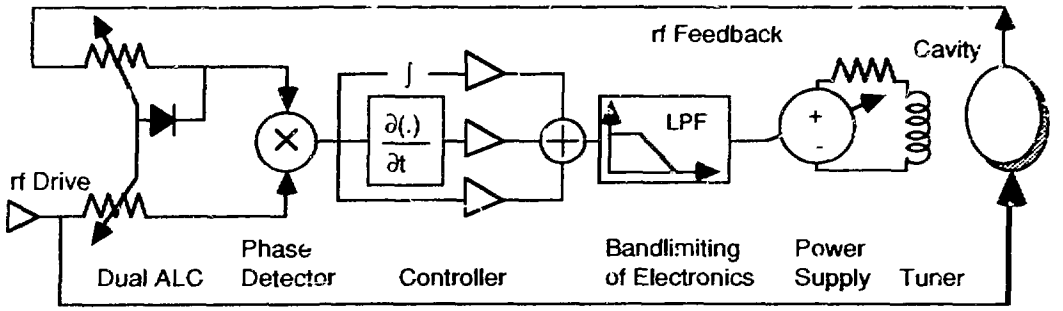

Figure 4-1: Resonance Feedback Loop

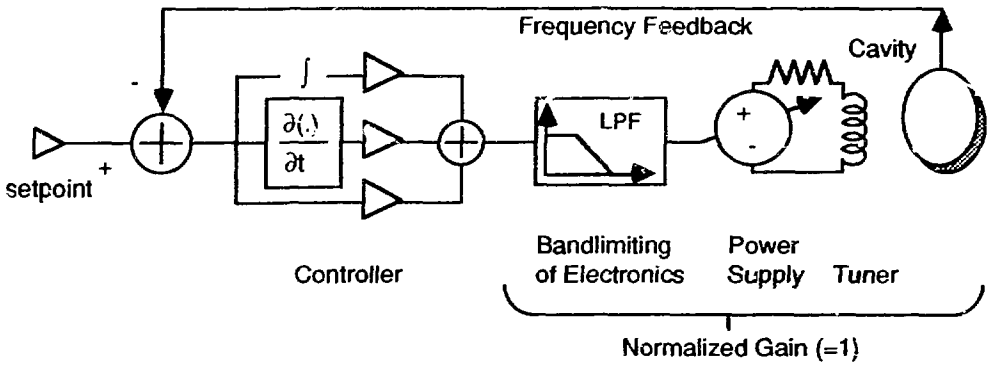

Figure 4-2: Linearized Model

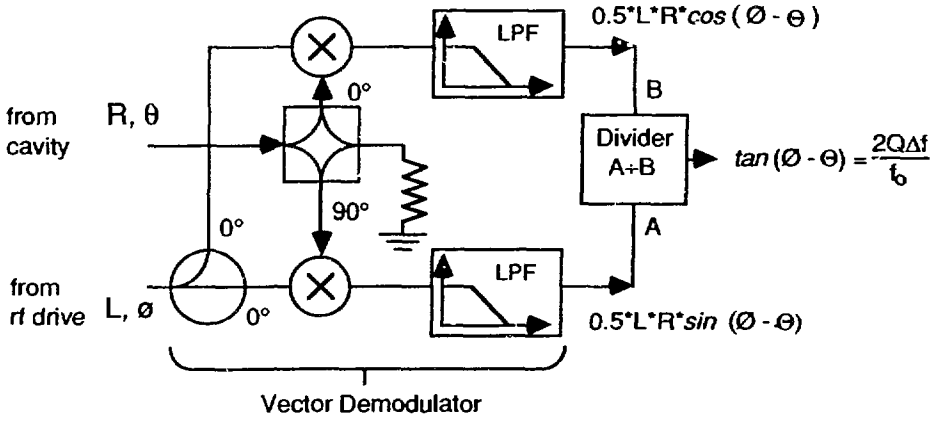

Figure 4-3: Alternate Frequency-Error Measurement

The characteristics of the model components are as follows:

Cavity	ω_0 responds instantaneously to tuner current
Tuner	corner frequency = R/L ≈ $2*10^{-3} \div 400*10^{-6}$ = 5 radian/s
Power Supply	$80*10^3$ radian/s corner frequency (see Appendix B)
Electronics	$6*10^6$ radian/s corner frequency – arbitrary.

Bode plots of the open-loop model, with and without a proportional-integral (PI) controller are shown in Figure 4-4. The controller shown is not the highest gain controller possible for the model. Rather, it provides significant gain and a reasonable margin for modeling error.

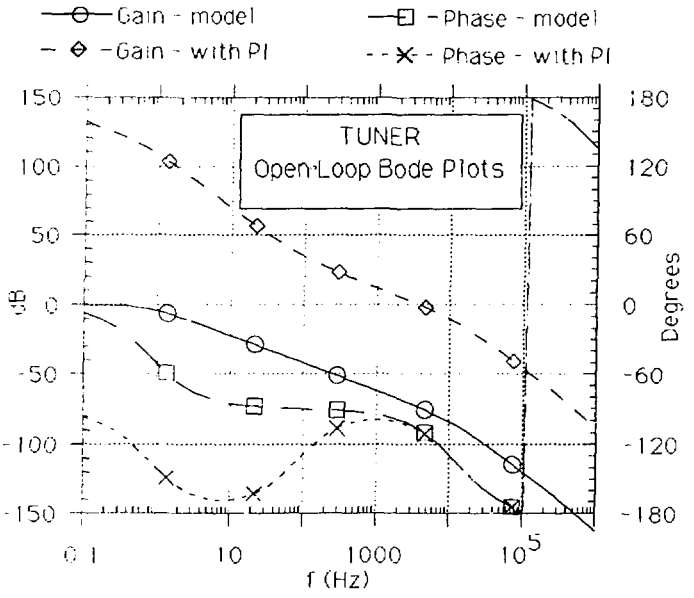

Figure 4-4: Open-Loop Bode Plots

Application of the "rule of thumb" that the gain-bandwidth product is a constant, predicts a closed loop bandwidth of ≈ 5 kHz. This bandwidth is significantly less than that of the fast-feedback loop; consequently, there should be little dynamic interaction between the resonance loop and the fast-feedback loop. Numerical simulation of the model confirms the bandwidth estimate and provides more information on the step and ramp response, as shown in Figures 4-5 and 4-6. For the plots in Figures 4-5 and 4-6, it is assumed that the solenoid current ranges over 0 to 2000 A for the full 15 MHz tuning range.

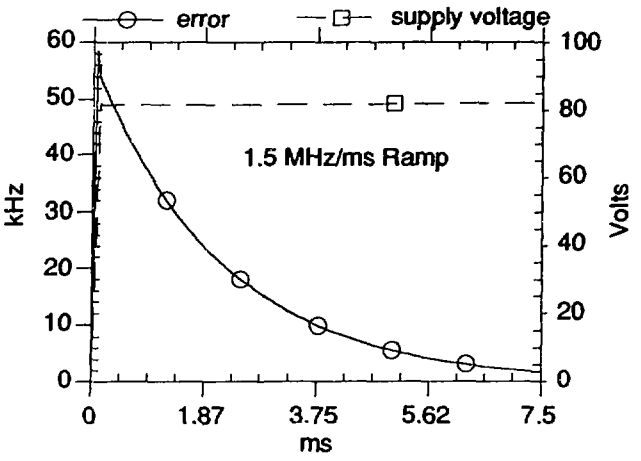

Figure 4-5: Ramp Response

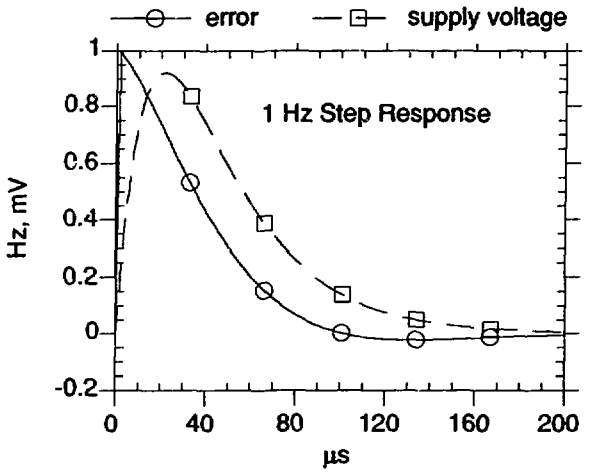

Figure 4-6: Unit Step Response

The ramp response indicates that feedback alone is definitely inadequate. Because the majority of required tuning current (as a function of time) can be predicted, some form of feedforward could be used. Thus, feedback would provide correction for feedforward inaccuracies only. The required feedforward accuracy can be estimated by noting that the error with feedback peaks at 60 kHz. If a 10° limit is placed on the ramp phase error, then the frequency error at this phase error is:

$$\Delta f = \frac{f_o}{2Q}\,\mathrm{Tan}(10°) \qquad (4\text{-}1)$$

$\Delta f = 1.1$ kHz for $f_o = 50$ MHz, $Q = 4000$.

Feedforward must provide a 60-fold error reduction; consequently, 98.3% of the tuning must be accomplished by feedforward. Such accuracy demands that the beam current magnitude be used to adjust the feedforward signal to provide beam loading compensation by detuning.

The step response shows that the 20% excess capacity specified for the power supply should ade-

bance, the fast-feedback loop will increase the drive power to compensate for the tuning error. A large tuning error would be produced upon beam injection. It is shown in §5.4 that the required power is greater than can be handled (on a continuous basis) by the 150 kW final amplifier. Anticipatory detuning can be used to reduce the peak power demand. By partially detuning the cavity prior to beam injection, the rf power demand is increased beyond the nominal on-tune case; however, this detuning reduces peak power demands during injection.

In conclusion, feedback control alone is incapable of achieving the desired performance. Accurate feedforward must be combined with feedback to be able to track the 10 ms frequency ramps. Even with such a controller, significant transients appear to be unavoidable during the injection (and ejection) of the beam at the start (end) of the acceleration cycle.

4.2 Tuner Model

Just two states comprise the continuous-time dynamics of the model: the power supply voltage and the solenoid current. It is assumed that all other components have a bandwidth in excess of 2 MHz so as to not interfere with loop dynamics. The majority of the simulation code deals with feedforward.

The feedforward controller design is based on that used with the ISIS synchrotron [6]. This controller is represented in the lower portion of Figure 4-7. Conceptually, feedforward modifies the setpoint by the inverse of the system dynamics. If an exact inverse is used, system output will match the setpoint. Due to the cyclic nature of the tuning operation, the feedforward signal can be recycled and the tuning error may be used for feedforward update. Convolution of the system inverse with the tuning error can be done using fast Fourier transforms (FFTs) without windowing or padding, again due to the tuner's cyclic operation. In the preliminary evaluation it was determined that accurate feedforward is required, yet the relationship between solenoid current and cavity resonance is quite non-linear (see Figure 2-4). This non-linearity conflicts with the use of a linear system inverse; therefore, prior to the convolution, the tuning error is multiplied by:

$\frac{\partial i_S(x)}{\partial f(x)}$, where $i_S(x)$ is the solenoid current expected at time x into a cycle

$f(x)$ is the expected cavity frequency at time x into a cycle.

(In Figure 4-7 'x' is shown as t modulus ('%') T_L, where T_L is the cycle period.)

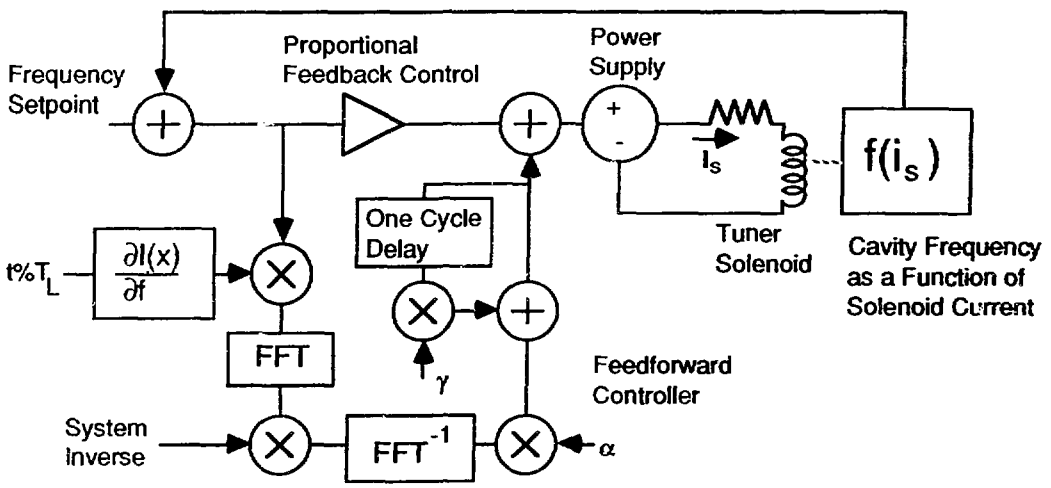

Figure 4-7: Tuner Simulation Block Diagram

The simulation user can specify:

- weighting of feedforward update (α and γ),
- a settling time during which update of the feedforward signal is inhibited,
- FFT record length,
- polynomials describing $f(i_S)$, and $i_S(f)$,
- separate linear systems: one defines the power supply and solenoid, the other is a similar (but not necessarily identical) system used to generate the system inverse, and
- proportional feedback gain.

Generation of an appropriate frequency setpoint is done by fitting a $\sin^2$ function to the first 10 ms of the expected f(t) function, as shown in Figure 4-8. A greater-than-required frequency range is used because it allows a smooth f(t) at the ends of the cycle, and it deviates on the side of a more difficult cycle to track. On average, the simulated frequency setpoint has a greater df/dt than required. Further, at the high-frequency end the simulated setpoint has a considerably steeper slope, where df/di_S is the lowest. For $t > 10$ ms f(t) is not specified.

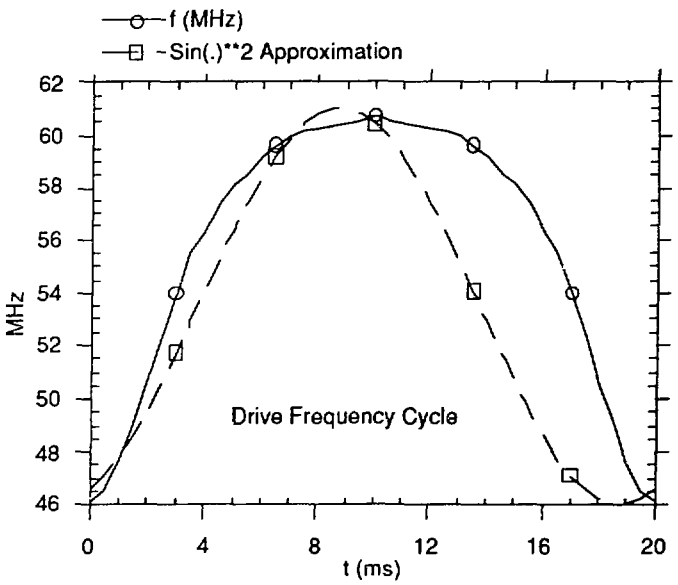

Figure 4-8: Frequency Setpoint Versus Time

4.3 Tuner Simulation Cases

Cases were run to find:

a) the largest proportional gain that doesn't create ringing in the response,
b) the minimum FFT record length,
c) appropriate weighting factors for feedforward update, and
d) the sensitivity of feedforward to errors in the system inverse.

The simulation showed:

a) Proportional gain, for the feedback controller, should not exceed 60 A/Hz.

b) Feedforward performance improved with increasing record length up to 512 points. Little improvement was observed with records of 1024 points.

c) With reference to Figure 4-7, stable feedforward update and rapid settling of the feedforward sequence was obtained with $\alpha = 0.9$ and $\gamma = 1.0$. Noise was not added to the frequency error signal; consequently, a smaller value for α would be judicious in an actual system. Forty milliseconds of operation with feedforward updates disabled is required to allow the start-up transient to die away. If this 40 ms hold-off is not used a transient is induced in the feedforward signal.

d) Sensitivity to errors in the system inverse appears to be tolerable. The performance goal is met despite varying the bandwidth of both the power supply and solenoid from 0.9 times to 1.25 times of that used by the system inverse. These cases are illustrated in Figure 4-9 as "Narrow-band" and "Wide-band", respectively. Traces labelled "Ferr" are the frequency errors, "Fseq" are the feedforward signals. Similarly, it was found that it is possible to meet the performance goal while keeping the system bandwidth fixed and varying the system inverse model by ±25%. Had an intolerable sensitivity been discovered, on-line measurement of system dynamics would be required.

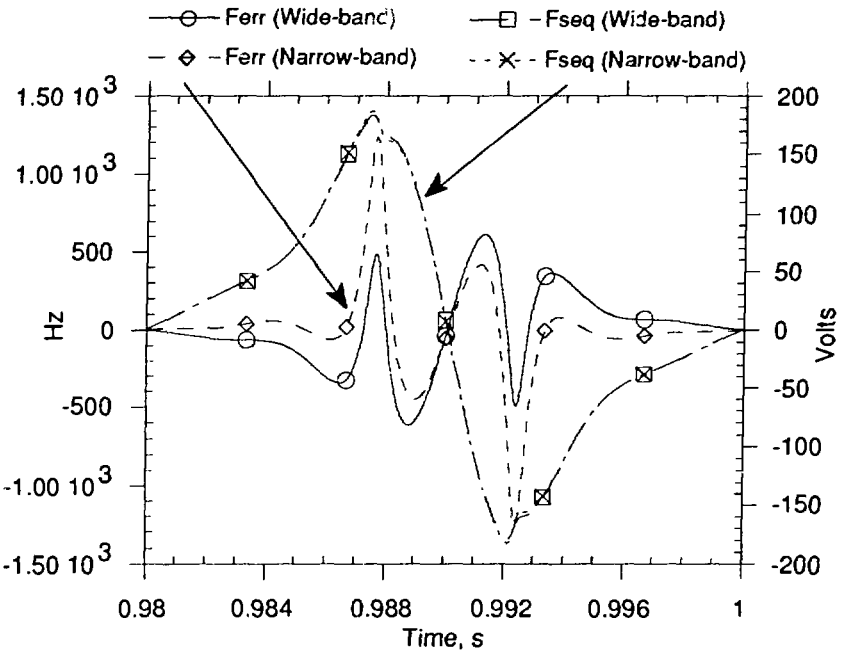

Figure 4-9: Performance with Erroneous System Inverse

Another comparison is illustrated in Figure 4-10. Here the bandwidths used to calculate the system inverse match the power supply and solenoid bandwidths. One case was run for 1 s, while the other was run for 50 more cycles to 2 s. Note that over the last 1 s the error has reduced only slightly. Further reduction would be unlikely.

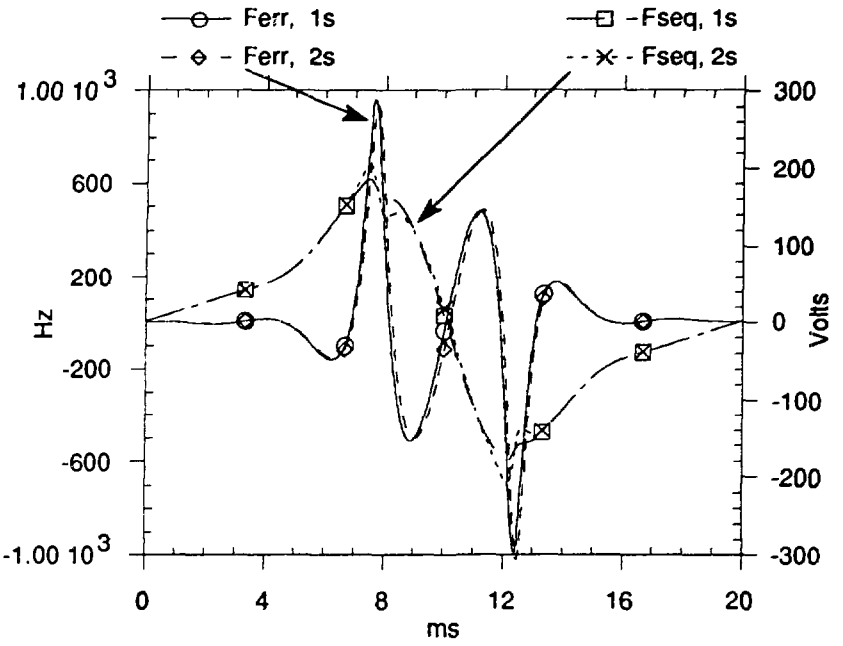

Figure 4-10: Comparison of 1 s and 2 s Operation

5.0 FAST LOOP

5.1 Initial Evaluation

5.1.1 Direct Fast-Feedback

Referring to the simplified fast-feedback loop shown below, the Laplace transfer function of the closed loop system is:

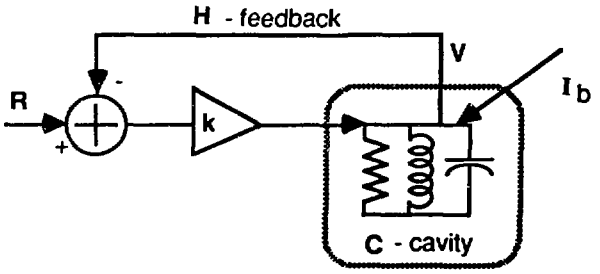

Figure 5-1: Simplified Fast-Feedback Loop

$$\frac{\mathbf{V(s)}}{\mathbf{R(s)}} = \left(\frac{1}{\mathbf{K(s)C(s)}} + \mathbf{H(s)} \right)^{-1} \qquad \text{where s is the Laplace variable} \qquad (5\text{-}1)$$

Without loss of generality, the on-resonance value of $\mathbf{C}(j\omega_0)$ can be normalized to $1\angle 0°$ and the magnitude of **H** taken as 1. For $|\mathbf{K(s)C(s)}| >> 1$,

$$\frac{\mathbf{Y(s)}}{\mathbf{R(s)}} \approx \frac{1}{\mathbf{H(s)}} \tag{5-2}$$

Similarly, the transfer function of V relative to $\mathbf{I_b}$ is:

$$\frac{\mathbf{V(s)}}{\mathbf{I_b(s)}} = \left(\frac{1}{\mathbf{C(s)}} + \mathbf{K(s)H(s)} \right)^{-1} \tag{5-3}$$

For $|\mathbf{K(s)C(s)}| >> 1$,

$$\frac{\mathbf{V(s)}}{\mathbf{I_b(s)}} \approx \frac{1}{\mathbf{K(s)H(s)}} \tag{5-4}$$

If one assumes that the average beam loading is compensated by use of detuning, then $\mathrm{Tan}(\psi) = Y$ and at the drive frequency, ω_d,

$$|\mathbf{C}(j\omega_d)| = \frac{1}{\sqrt{1+Y^2}} \approx \frac{1}{Y} \quad \text{for } Y >> 1 \tag{5-5}$$

Also $\angle \mathbf{C}(j\omega_d) = \psi$.

Therefore, while the proportion of v produced by the beam current relative to that of $\mathbf{i_p}$ is not affected by detuning, the amplitude and phase of the closed loop gain is affected. For example, for

$$Y = 20,\ \mathbf{K}(\omega_d) = 65\angle 0°, \text{ and } \mathbf{H}(\omega_d) = 1\angle 0°, \tag{5-6}$$

then $\psi = 87°$ and $\frac{\mathbf{Y}(\omega_d)}{\mathbf{R}(\omega_d)} = 0.94\angle 16.9°$.

The intent of the fast feedback loop is to compensate beam transients and errors in the resonance control detuning. Fast feedback reduces these transients by $\approx \mathbf{K(s)}$ times. The bandwidth of **K** can be made wider than the operating bandwidth of the Booster, so that $\mathbf{K(s)} \approx$ constant over the frequency band of concern (ignoring linear phase shift). Using the same example as above, if no compensation by way of detuning were done and unlimited final amplifier power was available, the error in v would be $\approx 4.6\%$ amplitude and 17°. Pre-detuning in anticipation of beam arrival would reduce this error.

It is unlikely that further reduction of transient disturbances can be achieved by increasing the open-loop gain, due to the stability limitations imposed by loop transit time and component bandwidth limitations.

In conclusion, although the proposed fast feedback will have a significant compensating effect, it alone will not be sufficient. Compensation by detuning and/or feedforward will be required if the steady-state error is to be adequately reduced.

5.1.2 Feedback Phasing

Referring to Equation 5-2, it can been seen that positioning a phase shifter in the feedback path, **H(s)**, would result in a 1:1 coupling of fast-loop phasing to θ_v. Placing the phase shifter in the forward path (as part of **K(s)**) would reduce this sensitivity by a factor of $\approx |\mathbf{K(s)C(s)}|$. This sen-

sitivity reduction drops off as the cavity is detuned. If detuning is such that the average beam current is compensated, then the phase sensitivity reduction is on the order of $|\mathbf{K}(s)| * Y^{-1}$.

An obvious but crucial point: if the resonance controller shares the feedback signal with the fast loop, then the physical location of the phase-shifting device must be after the point where the resonance controller samples the feedback signal.

The realization of phase adjustment impacts on control requirements. A device is desired that will shift the phase over 360° while neither adding to loop delay nor inducing amplitude modulation. Further, the phase shifter should be a low-distortion element, particularly if it is to be positioned in **H**(s). Various schemes have been considered.

The simplest approach is to utilize a commercially available lumped-element voltage variable phase shifter. Unfortunately, such devices typically have only a 10% bandwidth and have transmission delay times of ≈20 ns, making these devices unsuitable. The narrow bandwidth limitation could be overcome by up-converting, phase shifting, then down-converting (coherently).

A method proposed by Boussard generates a quadrature feedback signal by differentiation, followed by amplitude division by the drive frequency [7]. By weighting and then combining the in-phase and quadrature signals, an overall phase shift is achieved. The advantage of this method is that (mathematically) differentiation produces a quadrature signal independent of frequency. It is not clear how to implement frequency-independent differentiation at 50 MHz.

A circuit similar to Boussard's, but which avoids the need for differentiation, is one in which the differentiater is replaced by a 90° hybrid, as shown in Figure 5-2. Tests of a 90° hybrid show ± 0.25 dB and ± 0.2° variation over a 33% bandwidth (centred at 300 MHz[1]). Transit time through the device is less than 1 ns. This circuit appears to be the most straightforward solution.

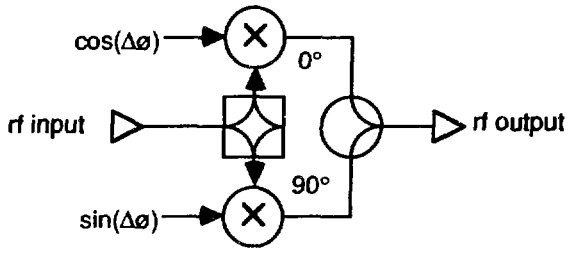

Figure 5-2: 90° Hybrid Base Phase Shifter

Because the objective is to have the correct phase delay of the fast-feedback loop, an intuitive approach would be to control the phase using a feedback controller that derives its error signal by mixing the reference and error signal to detect the phase error between the reference and feedback:

[1] A 50 MHz hybrid was not available. It is assumed that the properties of the hybrid will scale to 50 MHz.

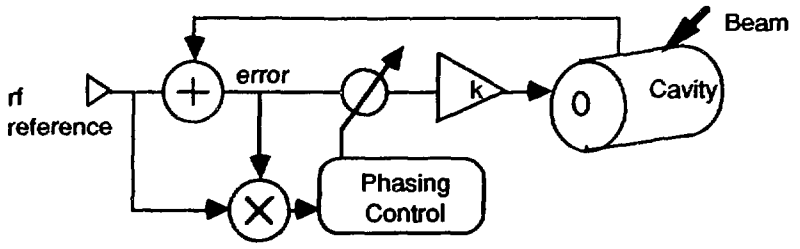

Figure 5-3: Mixing Approach to Feedback Phasing

The error signal is used instead of the feedback signal because the latter would be insensitive to phasing errors by virtue of the fast feedback, which attempts to keep this signal in phase with the reference.

Unfortunately, use of phase detection for feedback control of the fast-feedback phasing would result in 1:1 coupling between the resonance controller and loop phase. For example, if the tuning was such that v lagged the final amplifier current, i_p, by 10° then the feedback phasing loop would incorrectly advance the feedback phase by 10°. While this false phase correction would actually reduce the sensitivity of the closed loop gain to ψ, fast-feedback stability would be compromised.

The tuner-phasing coupling could be reduced by using significantly different response times for the two loops, and/or by using multivariable control. It is not clear that the response times can be made to be adequately different and multivariable control represents a considerable complication.

Instead of tackling the phasing problem with feedback, correct phasing can be accomplished by applying a predetermined frequency-to-phase transformation on the rf reference frequency (as shown in Figure 2-2). Such a scheme requires that an accurate measure of this frequency be available. This frequency feedforward signal is also required for the tuner; hence, its use with the phasing control should demand only incremental costs. If one assumes that a frequency feedforward signal is available with ±100 kHz (±0.67% on 15 MHz) accuracy, then the phase could be controlled to within ±2.5°, provided the phase-shifting circuit bandwidth is ≥ 5 kHz (see Appendix B).

5.1.3 Baseband Fast-Feedback

An alternative to direct fast-feedback, and the corresponding feedback phasing, is baseband fast-feedback. Baseband feedback resembles direct feedback, except the summing junction is replaced by the circuit shown in Figure 5-4.

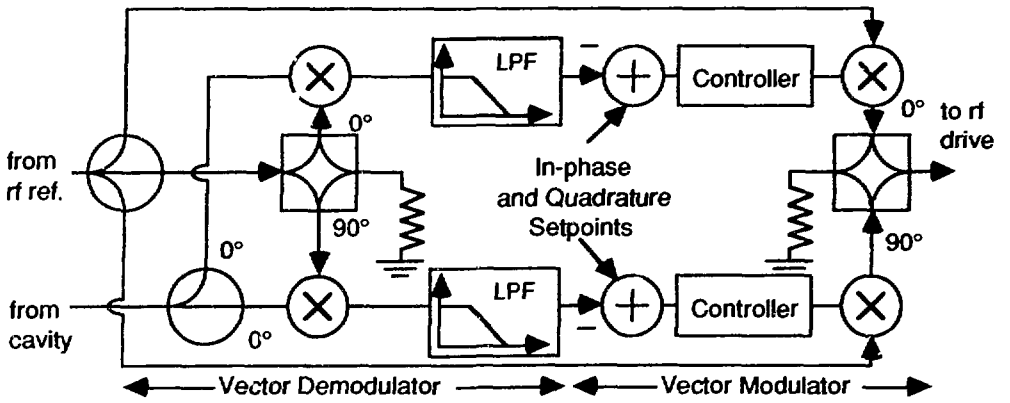

Figure 5-4: Coherent Demodulation/Modulation

The rf reference is split using a 90° hybrid. Both hybrid outputs are used to down-convert (demodulate) the cavity feedback signal; thus, the feedback signal is converted into baseband in-phase and quadrature signals. The down-converted signals are subtracted from setpoints and the resulting error signals are amplified by identical controllers. Controller output is then up-converted (modulated) by the reference and the rf signals are re-combined in quadrature.

Note that direct feedback is equivalent to baseband feedback when the in-phase setpoint controls the desired amplitude, the quadrature setpoint is zero, and the reference signal is of constant amplitude. The advantage of the baseband method is that loop stability is independent of feedback phasing. Changes in feedback phase are seen as a rotation between the in-phase and quadrature components; therefore, feedback phase affects the relationship between reference phase and cavity-field phase. While this behaviour differs from that of direct feedback, the net effect is simply to make the cavity appear to be physically located at a greater distance from the feedback summing junction.

Another potential advantage of the baseband method is that the controller is operated at lower frequency relative to direct feedback. This allows greater flexibility of controller design.

5.1.4 RF Feedforward

RF feedforward can be useful to correct the average beam current on a time scale that is shorter than the tuner response. Feedforward uses knowledge of the beam arrival time and amplitude so that a cancelling current can be generated to coincide with the beam arrival at the cavity. Note that under steady-state conditions, with a full ring, feedforward would not be used because the average beam current would be compensated by the tuner.

Of the 45 total Booster buckets, five consecutive buckets will be left empty. Thus, there will be a 100 ns gap every 1 μs. Using a fast-feedback gain of 65 and a cavity Q_L of 4000, the system time constant ("e-folding" time) would be ≈ 390 ns. If feedforward was not used during these 100 ns gaps, the error in v would build to $100 * \left(1 - e^{-\left(\frac{100}{390}\right)} \right) = 23\%$ of the steady state feedback-only error. Using the example of equation 5-6, v would deviate as if Y = 0.23*20 = 4.6, giving 0.25% amplitude and 4° phase error. This estimate ignores loop transit time, which would reduce the capability of fast-feedback; consequently, it would be judicious to provide feedforward control during the empty bucket intervals.

5.2 Fast-Loop Model

Baseband fast-feedback was not simulated, because the fast-loop was examined at fixed frequencies and 'correct' feedback phasing. Under these conditions, the two methods are equivalent.

The fast-loop model consists of delay lines, an rf drive chain, a final amplifier and cavity, and bandlimited feedback. The final amplifier is split into linear and non-linear sections. The linear section is given in Figure 5-5 [8]. Plate current, i_p, is determined by the non-linear portion of the model. The components grouped as Zp model the final amplifier, Zc is the coupling capacitor between the tube and the cavity inner conductor, and Zg is the model of the cavity.

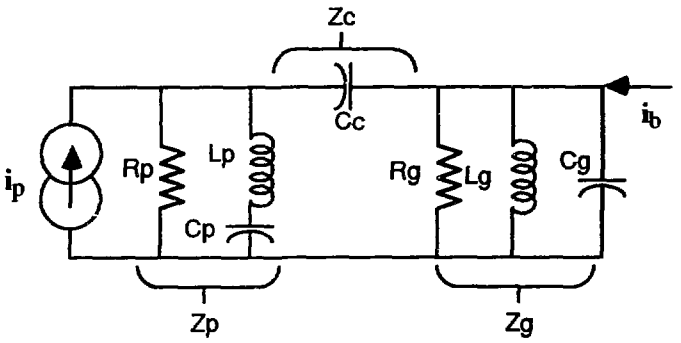

Figure 5-5: Final Amplifier and Cavity Model – Linear Portion

Plate capacitance measurements made at TRIUMF varied from 133 pF at 46 MHz to 200 pF at 61 MHz [8]. This can be modelled as an 88 cm open transmission line of $Z_o = 29\ \Omega$. Also, a close approximation is the series combination of 34.6 nH and 100.7 pF, as illustrated in Figure 5-6.

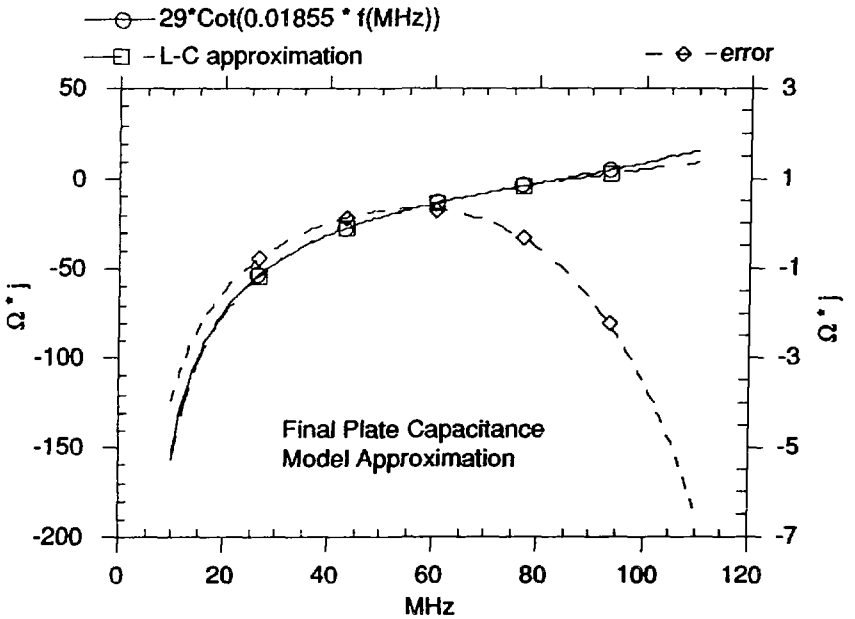

Figure 5-6: Plate Reactance Versus Frequency

Component values used for the final amplifier and cavity are as follows:

Rp = 8220 Ω	Cp = 100.65 pF Cc = 50 pF	Lp = 34.55 nH
Rg = 186.8 kΩ	Cg = 50 pF	Lg = 135 nH (@46 MHz) to 75 nH (@61 MHz)

Non-linear amplification is modelled using a third-order polynomial with coefficients that are a linear function of plate voltage. These coefficients were estimated using the tube manufacturer's constant current plot for the final amplifier (a 4CW150,000E). Because only one tube is used, i_p is cut-off for inputs less than zero. During heavy beam loading tube operation is centred around an 18 kV dc plate bias. The input-output relationships at the plate voltage extremes are shown in Figure 5-7.

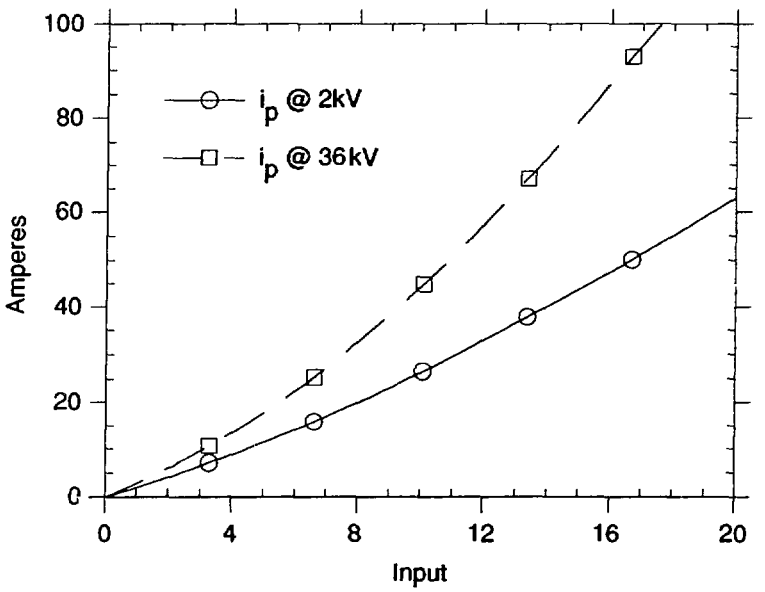

Figure 5-7: i_p Versus Input Drive and Plate Voltage

Both the rf drive chain and the feedback dynamics are modelled using second-order linear systems. These two systems, as well as the final amplifier and cavity system, were solved using a standard Fortran module called 'obcan' (for observer canonical form). This module implements a linear system (as specified by a Laplace polynomial) using the state assignment of the observable canonical form. For the linear system

$$\frac{C(s)}{U(s)} = \frac{b_m s^m + b_{m-1} s^{m-1} + \ldots + b_0}{s^n - a_{n-1} s^{n-1} - \ldots - a_0} \qquad (5\text{-}7)$$

the observer canonical form is shown in Figure 5-8.

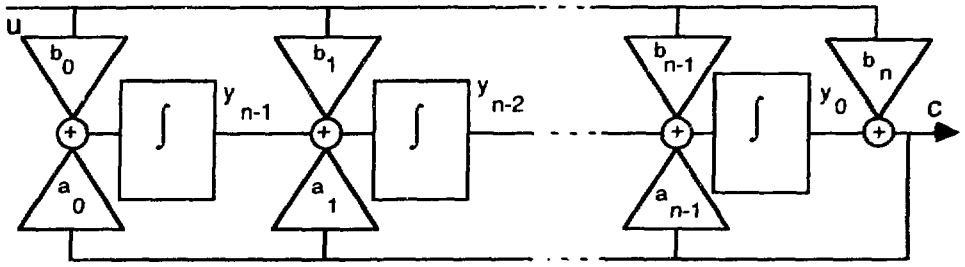

Figure 5-8: Observable Canonical Form

A 30 MHz to 85 MHz bandpass filter is used to model the rf drive response. An under-damped lowpass filter is used for the feedback dynamics. A damping factor of 0.5 and a 3 dB bandwidth of 640 MHz is used.

Three fourth-order Padé delay approximations are used to model loop transit time. Two Padé delays are specified by input data. The third is set, by an initialization procedure, to ensure a loop phase of 0 or 180°, whichever requires the least additional delay to achieve. The linear expression for the fourth order approximation is:

$$\mathbf{P}_4(s) = \frac{1 - (Ts/2) + (3/38)(Ts)^2 - (1/84)(Ts)^3 + (1/1680)(Ts)^4}{1 + (Ts/2) + (3/38)(Ts)^2 + (1/84)(Ts)^3 + (1/1680)(Ts)^4} \qquad (5\text{-}8)$$

where, T is the delay time.

While the 'obcan' subroutine could be used to model the time delays, a separate subroutine is used that uses T to generate the required coefficients for integration.

The ensemble of the model components is illustrated in Figure 5-9. The 'Sign' parameter shown in Figure 5-9 is set to either +1 or -1, corresponding to a loop phase of 180° or 0°, respectively.

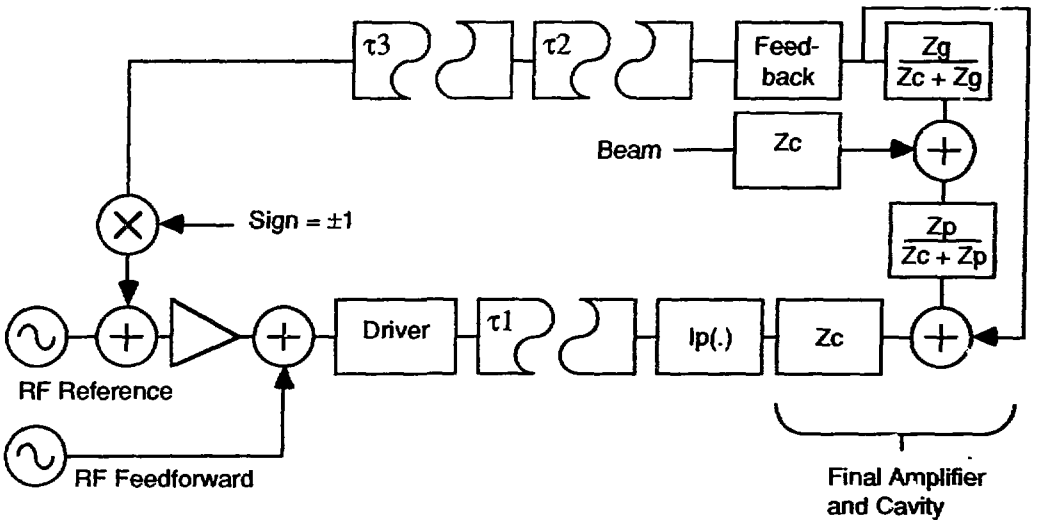

Figure 5-9: Overall System Block Diagram

If one ignores the final amplifier non-linear gain by setting it to 1.0, an open loop Bode plot can be generated from the model linear systems, as shown in Figure 5-10. In Figure 5-10, loop transit

time is set to 40 ns to obtain correct feedback phasing. A delay of 70 ns was used during the simulation cases.

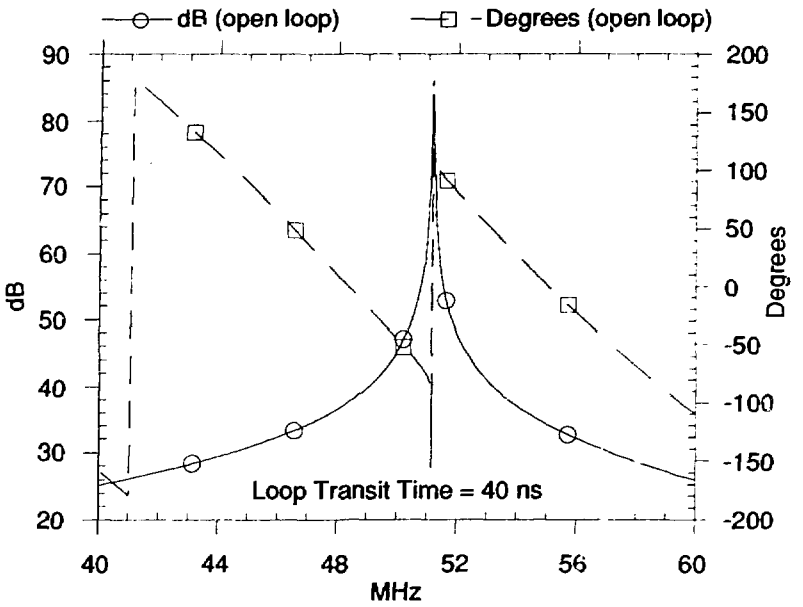

Figure 5-10: Overall Bode Plot

A one-half sinusoid wave-shape is used to model beam current. Peak current is found from the Fourier expansion of such a wave-shape, giving:

$$\text{peak current} = \frac{\pi C f_o}{40} \quad \text{where: C is the total charge in the 40 filled buckets,} \qquad (5\text{-}9)$$

f_o is in Hz.

5.3 Oscillatory Initialization

"Steady state" for this system is a constant amplitude, constant frequency sinusoidal oscillation; hence, phasor circuit analysis provides a convenient means of initialization. Initialization consists of determining the input and output of a module, and then determining each of the internal states. The initialization procedure begins with a specified v, works backward through the forward path to the summing junction, then forward to the summing junction through the feedback path. For each module, equation 5-7 is calculated with $s = j\omega$, where ω is the given operating frequency. This calculation produces a single complex number relating the amplitude and phase of the output of a module to its input. The actual signal value is the real part of the inputs and outputs calculated in this manner.

Given the input and output (complex value), the internal states are found by working through Figure 5-8, calculating one state at a time in complex form, then assigning the real part of the result to the simulation state. In phasor analysis, integration is equivalent to multiplication by $(0 - j/\omega)$. For example:

$$y_{n-2} = (0 - j/\omega)(y_{n-1} + u*b + c*a_2) \qquad (5\text{-}10)$$

5.4 Fast-Loop Simulation Cases

Fast-feedback performance is summarized in Table 5-1. Further details for each case listed in Table 5-1 are given below, along with plotted waveforms. The Δ Error and Tube Dissipation columns of Table 5-1 require explanation:

Under steady-state beam-loaded conditions, cavity voltage will differ from the no-beam case due to controller limitations. The desired voltage could still be obtained by adjusting the rf reference. Errors produced from beam-loading transients would then dominate voltage deviations as seen by the beam. As a measure of this deviation, the Δ Error column lists the change in voltage error during the passage of five empty buckets.

Peak power dissipation in the final amplifier is estimated from the peak value of i_p and by assuming that this current is in quadrature to the plate voltage. Power dissipation can then be calculated from:

$$P = \frac{|i_p|_{peak}}{2\pi} \int_0^{\pi} \cos(x)(Vdc + Vac*\sin(x))dx \qquad (5\text{-}11)$$

$$P = \frac{|i_p|_{peak}}{2\pi} [2*Vdc + 0]$$

$$P = \frac{|i_p|_{peak}}{\pi} * Vdc \qquad \text{,where:} \quad \begin{array}{l} Vdc \text{ is the plate bias voltage,} \\ Vac \text{ is the plate rf voltage swing.} \end{array}$$

Table 5-1: Case Comparison

Case	Setpoint |v| kV, f_0 MHz	θ_s	Control Action	Error	Δ Error	Tube Dissipation	Figure
1	0, 51.173	0°	none	20 kV/μs,	N/A	N/A	5-11
2	62, 51.173	22°	feedback	0.33%, 4.6°	0.27%, 2.8°	195 kW	5-12
3	32, 61.166	0°	feedback	2%, 11.5°	1%, 3.2°	260 kW	5-13
4	32, 61.166	0°	feedback, detuning	0.75%, 7°	0.25%, 1.25°	110 kW	5-14
5	32 61.166	0°	feedback, feedforward	0.14%, 3°	0.07%, 0.9°	275 kW	5-15

In all cases: beam charge = 1.92 μC, 40 buckets filled, 5 buckets empty,
loop transit time ≈ 70 ns

Performance Goal: $|\Delta v|/|v| \leq 0.3\%$ rms and $|\Delta\theta_v| < 2.3°$ rms

Findings from the simulation are:

- With reference to cases 2 and 3 in Table 5-1, it is confirmed that feedback alone is not capable of meeting the performance requirements, even if unlimited rf power was available.
- Detuning for compensation of the average beam current is required for the purpose of power dissipation in the final amplifier. This can be seen by comparing cases 2 and 3 to case 4 of Table 5-1.
- Feedforward control is not required, but is capable of significantly improving performance. Cases 4 and 5 (of Table 5-1) illustrate the effect of feedforward.

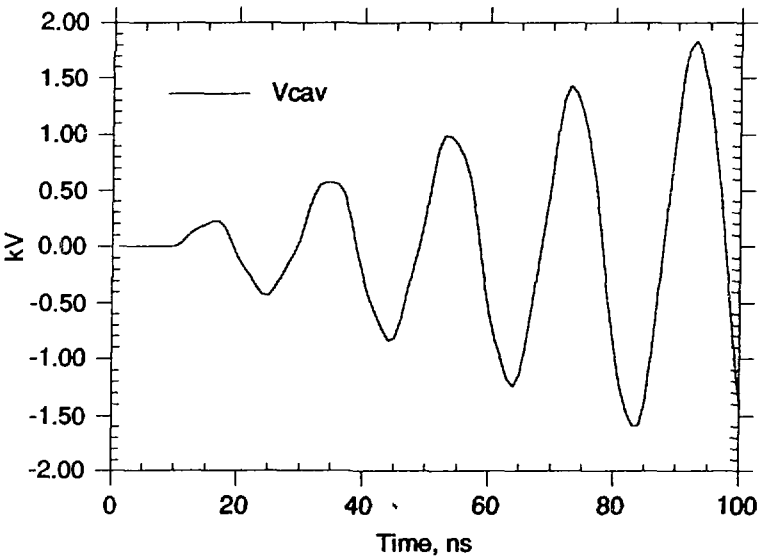

Figure 5-11: Beam-induced Voltage, no RF Drive

Figures 5-12a,b present the cavity voltage (v), voltage error and plate current during the passage of five empty buckets. The 62 kV amplitude and mid-band 51 MHz frequency setpoint make this a mild case with a quadrature beam loading factor of 11. Note that the error voltage is essentially always at 90° to the desired cavity voltage; hence, despite the rather large error amplitude, the deviation in the amplitude and phase of v is quite small.

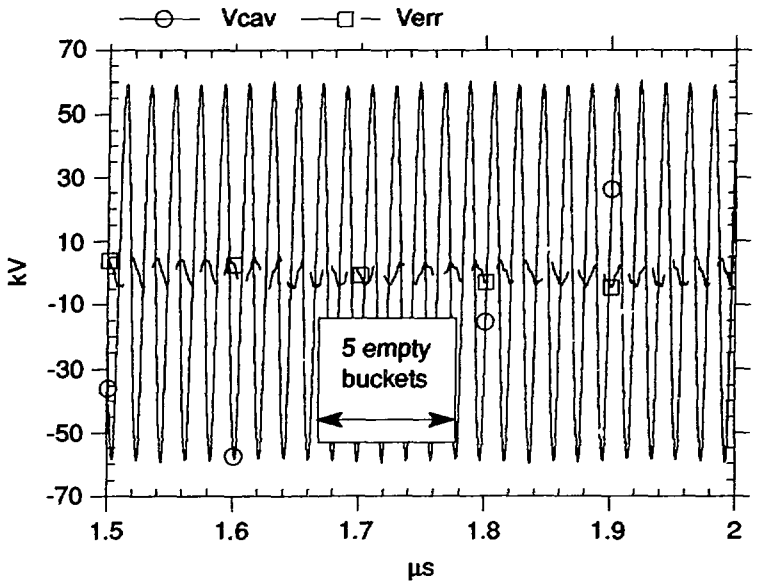

Figure 5-12a: 51 MHz Feedback Case, Cavity Voltage and Error

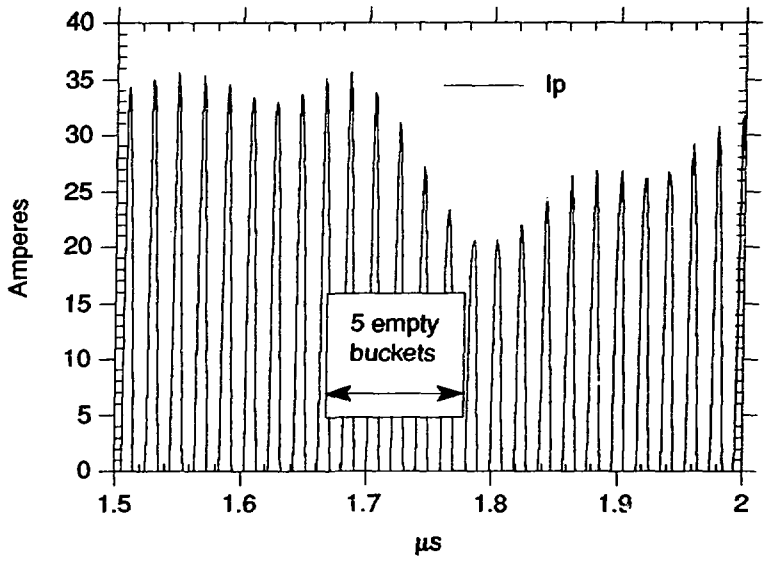

Figure 5-12b: 51 MHz Feedback Case, Plate Current

For Figures 5-13a,b the case of Figures 5-12a,b was repeated at 61 MHz, $\theta_s = 0°$. This is the most extreme case, with a beam loading factor of 27. Beam current has increased by 20% (due to the higher frequency). Correspondingly, voltage error (Verr) is 20% greater, and in phase with the beam, as is the previous case. Plotted in Figure 5-13c is the result of down-converting v for use with a baseband fast-loop. For down-conversion, $\cos(2\pi*61.66*10^6*t)$ and $\sin(2\pi*61.66*10^6*t)$ were used in the mixing operation. The phase of these signals relative to v is arbitrary, but convenient in that the beam is nearly in phase with the sin(.) (quadrature) component.

The equivalence of the direct and baseband methods can be demonstrated by converting selected points into polar format. From Figure 4-13c, the maximum quadrature amplitude is -22.5 kV, and the minimum is -20.8 kV. The corresponding in-phase components are -26.6 kV and -27.4 kV. In polar form, these points are: 34.8 kV $\angle$-139.8° and 34.4 kV $\angle$-142.8°, giving a 1% change in amplitude and 3° change in phase. This is in good agreement with the 1% and 3.2° found in Figure 5-13a.

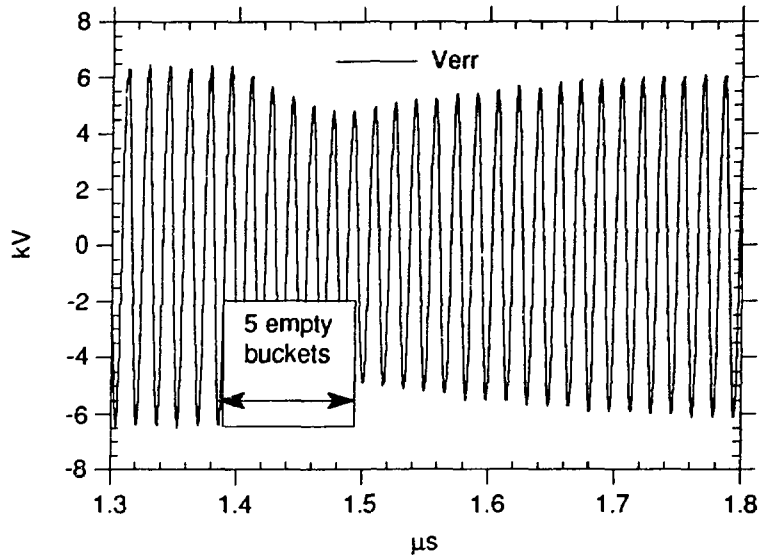

Figure 5-13a: 61 MHz Feedback Case, Voltage Error

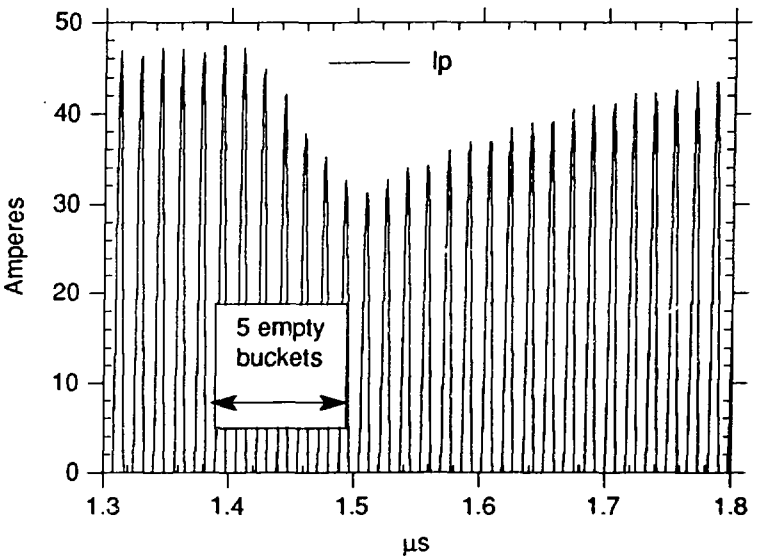

Figure 5-13b: 61 MHz Feedback Case, Plate Current

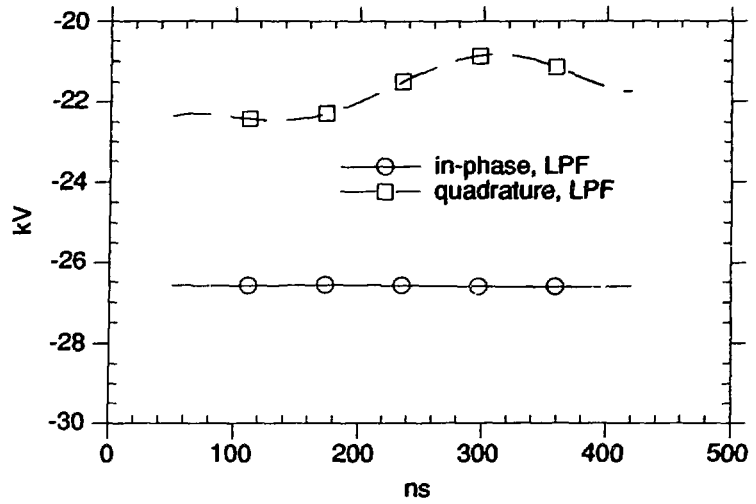

Figure 5-13c: Baseband (Down-Converted) Cavity V

The effect of detuning is demonstrated in the cases of Figures 5-14a,b. Simulated detuning is done manually by changing the cavity inductance from case to case until an approximate beam-loading compensation is achieved. The case shown in Figures 5-14a,b corresponds to $\Psi = 84.2°$ rather than the 87.9° that fully compensates for $Y = 27$; consequently, while i_p is significantly reduced, it is still a factor of $\tan(87.9°)/\tan(84.2°) = 2.77$ times greater than the nominal no-beam case. In addition to reducing the power demand, both the absolute error and error transient are reduced.

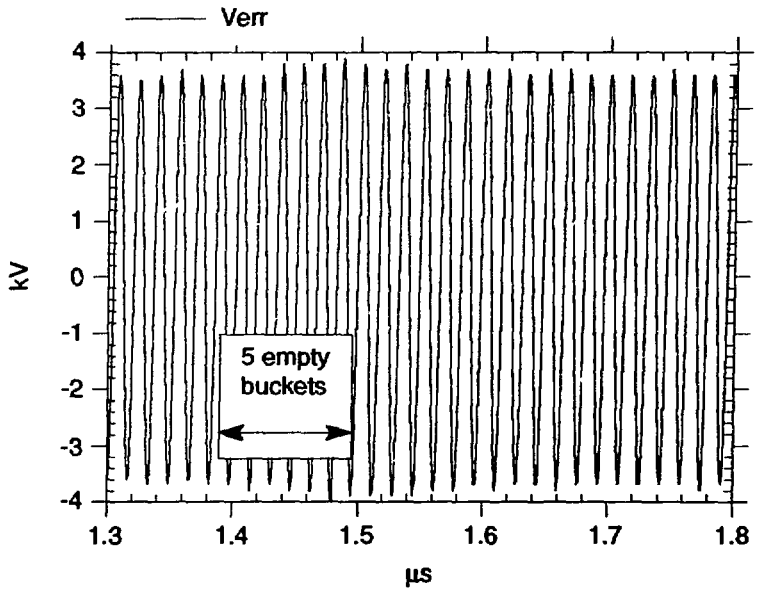

Figure 5-14a: 61 MHz Detuned Feedback Case, Voltage Error

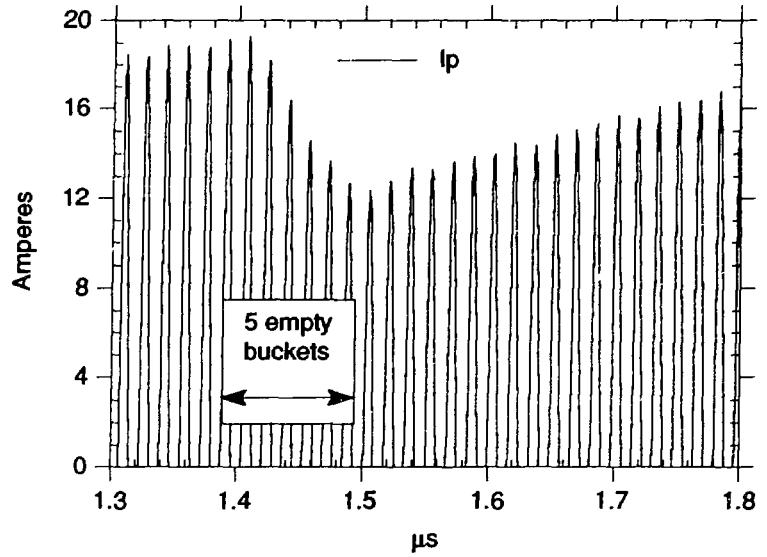

Figure 5-14b: 61 MHz Detuned Feedback Case, Plate Current

A combination of feedforward and feedback is illustrated in Figures 5-15a,b. Feedforward phase and amplitude were set, using trial and error, to within 10° and 10% of optimum by running cases with feedforward control alone. Feedforward synchronization with the beam was arbitrarily set at one-half cycle advanced, to partially correct for the drive chain transit time. As can be seen in Figure 5-15a, the voltage error has been reduced by a factor of four over the feedback-only case. This improvement has been gained with imperceptible change in i_p, as seen in Figure 5-15b.

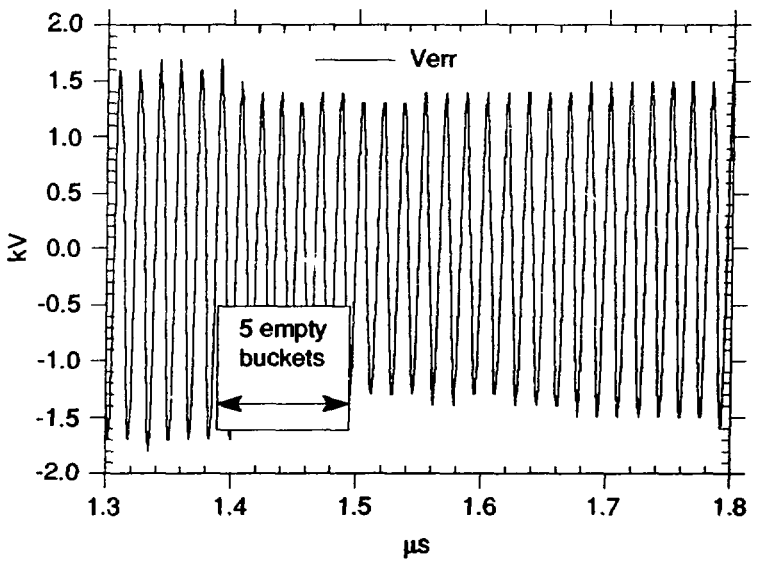

Figure 5-15a: 61 MHz Feedforward and Feedback, Voltage Error

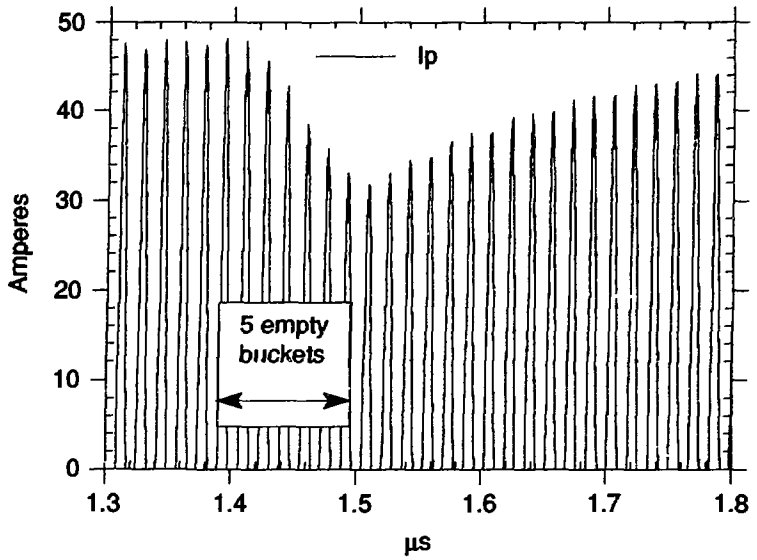

Figure 5-15b: 61 MHz Feedforward and Feedback, Plate Current

6.0 DESIGN OUTLINE

The basic hardware implementation is outlined in this section. The controller is sub-divided into functional blocks. For each block, a possible implementation is given and specific components are selected to demonstrate feasibility (not as a product endorsement). RF components selected assume a nominal operating power of +10 dBm.

6.1 Overall Controller

Figure 6-1 illustrates the functional sub-division and the inter-connections between these blocks. Functionally simplest is rf feedforward. RF feedforward consists of a 2-way power combiner just prior to the input to the rf drive chain.

A baseband fast-feedback loop is formed by: the vector demodulator, the dual-channel baseband controller, the vector modulator, the rf drive chain and cavity, and the feedback of a sample of the cavity fields. A dc block in the feedback path prevents the formation of a ground loop. The Mini-Circuits TMO1-1T 1:1 transformer can be used as such a dc block.

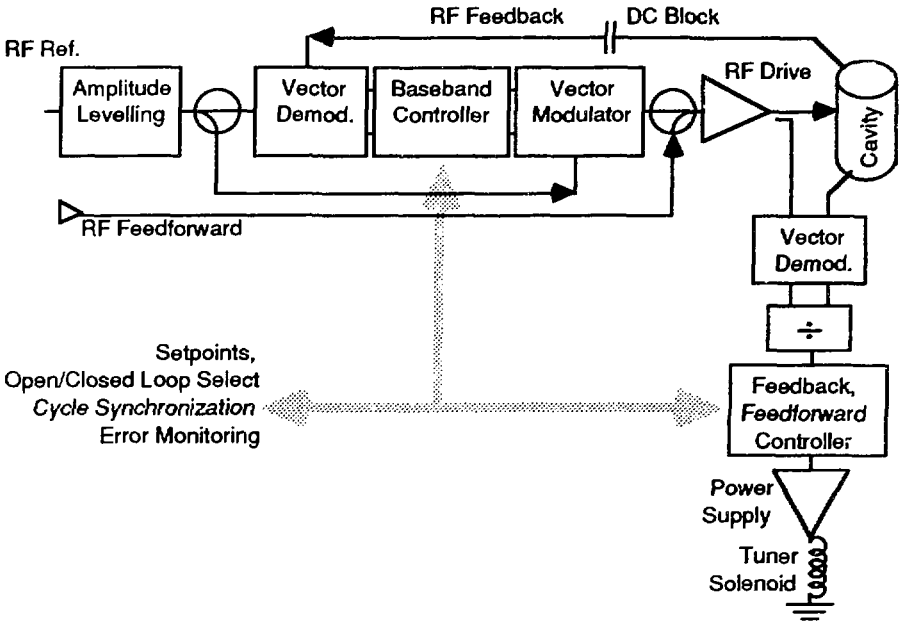

Figure 6-1: Overall Controller Hardware Configuration

A constant amplitude rf reference is produced by the amplitude levelling block. Thus, variations in input rf amplitude do not affect the amplitude of the cavity fields.

A vector demodulator and analog divider process the rf drive and cavity fields to produce a measure of tuning frequency error. Because of the large proportional loop-gain, a wideband analog divider must be used. The Analog Devices AD539, with a 15 MHz bandwidth, is an example of such a divider. The feedback, feedforward controller implements the proportional feedback control and adaptive feedforward tuning algorithm. Feedforward control must be synchronized with the acceleration cycle. A synchronization pulse is included for this purpose.

6.2 Amplitude Levelling

Levelling can be achieved by limiting (chopping) the rf input, then filtering to remove the harmonics generated by limiting (see Figure 6-2). A small signal amplifier following the limiter can be used to regain the power loss resulting from the limiting operation.

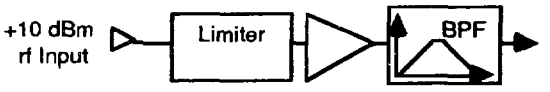

Figure 6-2: Amplitude Levelling

A possible device sequence is:

limiter	Watkins-Johnson WJ-L2 (0 dBm output for +7 to +20 dBm input)
amplifier	Mini-Circuits MAN-1HLN (10 dB gain, 3.7 dB NF)
filter	Mini-Circuits PLP-100 (100 MHz lowpass) and PHP-50 (41 MHz highpass)

6.3 Vector Modulator/Demodulator

The same vector demodulator design may be used for both the tuner and fast-loop applications. Care must be taken to remove mixing images without adding to the group delay over the frequency band, where loop gain is >0 dB. Mixing images must be removed, otherwise they will be amplified by the proportional gain, resulting in significant harmonic distortion. A limit of 10° phase rotation in the 0 to 2 MHz band (after demodulation) will not seriously erode loop-phase margin. Specifically, at 2 MHz from f_0, the fast-loop gain is -10 dB. Similarly, for the tuner loop, the gain is below -60 dB.

In the circuit shown in Figure 6-3, image rejection is achieved by use of an "image-rejection" mixer followed by a lowpass filter. "Image-rejection" mixers can typically provide 30 dB rejection when assembled for 1° and 0.5 dB balance. A third-order 30 MHz Chebyshev lowpass filter would further reduce the image by >30 dB, while adding only 7.5° rotation in the 2 MHz band.

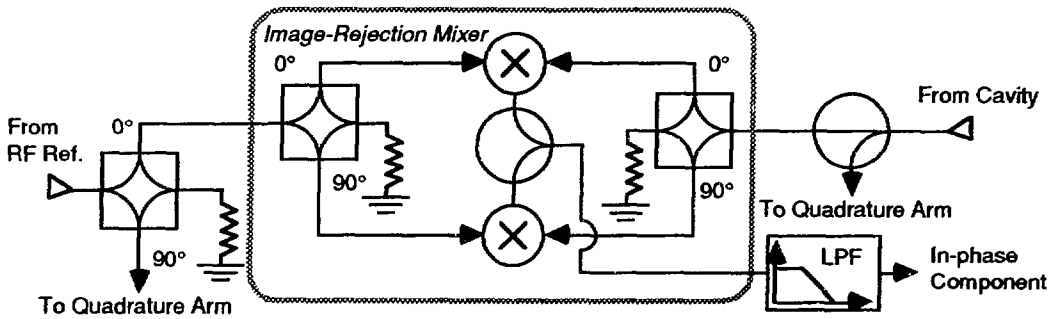

Figure 6-3: Vector Demodulator – One of Two Channels

Vector modulation can be implemented as shown in Figure 6-4. The rf reference is split into in-phase and quadrature components using a 90° hybrid. Voltage-controlled attenuators weight each rf component by the desired in-phase and quadrature amplitudes. The weighted signals are then summed by a 0° combiner. Variable attenuators are used rather than mixers, because less harmonic energy is produced. Also, attenuators are available that have a linear control response over adequate dynamic range.

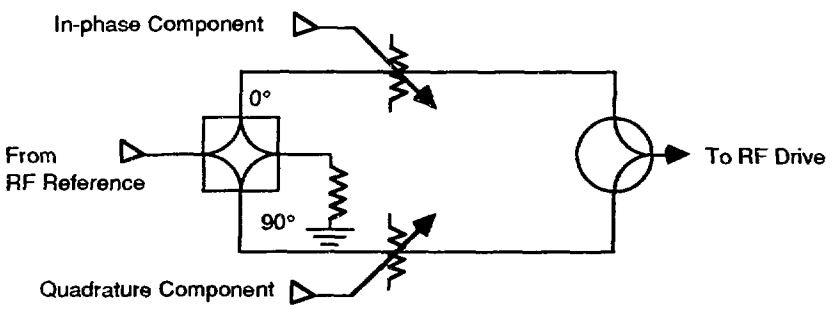

Figure 6-4: Vector Modulator for Baseband Feedback

Suitable components are:

90° hybrid	Merrimac QHS-3K-53B, f_0 = 53 MHz, 30% bandwidth, 3° and 0.3 dB balance.
power combiner	Mini-Circuits PSC-2-1, 3° and 0.2 dB balance.
variable attenuator	Anzac AT-101, 50 dB dynamic range, <3° phase variation over attenuation range, linear control response over 15 dB range.
vector phase detector	Merrimac IQP-3R-53B, f_0 = 53 MHz, 30% bandwidth, 2° and 0.3 dB balance.
lowpass filter	K+L Microwave Inc. series FL142, 30 MHz bandwidth, 0.5 dB passband ripple, 3rd order Chebyshev. (This filter will have only 7.5° phase shift from d.c. to 2 MHz. Attenuation at 92 MHz is 30 dB.)

6.4 Baseband Controller

A single channel of the baseband controller is shown in Figure 6-5. In closed loop operation, the demodulated cavity voltage is subtracted from a setpoint and amplified. When operating in open-loop mode, the setpoint is passed through the controller without alteration. Analog multipliers determine the mix of open and closed loop operation. A multiplier is placed in the output of both the open loop and the closed loop paths. An analog loop selection voltage controls the 'gain' of each path prior to summing.

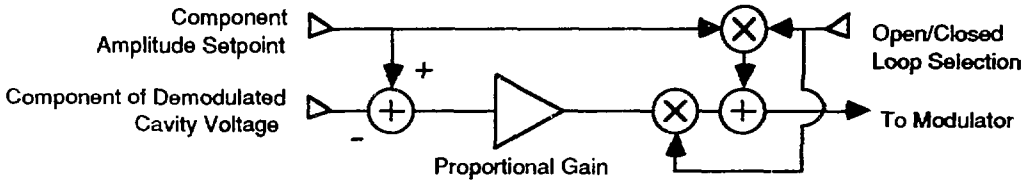

Figure 6-5: Baseband Fast-Feedback Controller (One Channel)

Example components are:

summing junctions and gain	National LM6365 amplifier and LM6321 buffer. The amplifier has a gain-bandwidth product of 400 MHz and a slew rate of 180 V/μs. The buffer is capable of driving 50 Ω with a bandwidth of 30 MHz and a slew rate of 555 V/μs,
analog multiplier	AD539 (60 MHz signal bandwidth in multiplier configuration).

6.5 Feedback and Adaptive Feedforward Controller

A sketch of the feedback and feedforward tuner controller is given in Figure 6-6. Open-loop operation is the simplest to realize. At all times, the open-loop setpoint is passed through to the controller output. Multipliers, which are in-line with the feedback and feedforward arms of the con-

troller, determine the strength of closed loop control. Multiplication by zero allows entirely manual control.

Both automatic controllers use an offset frequency error as input. This offset provides a means of correcting for inaccuracies in the frequency error measurement and/or to force a tuning offset.

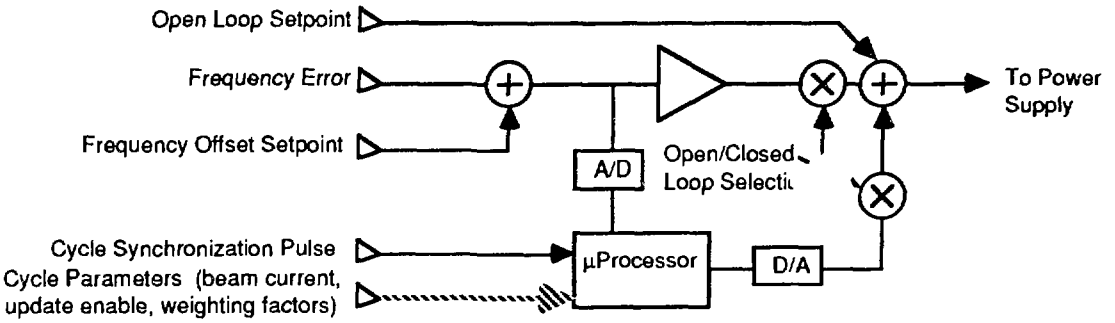

Figure 6-6: Feedback & Feedforward Controller

The feedback controller consists simply of a wideband amplifier. The feedforward controller consists of an analog to digital converter (A/D) a programmable digital processor, and a digital to analog converter (D/A). The processor must also interface to a supervisory computer so that it may obtain parameters (e.g., update weighting factors, beam current amplitude), and for enabling/disabling of the update operation. For each cycle, a synchronization pulse triggers the start of the feedforward sequence.

Processing demands are estimated using the worst-case assumption that the system inverse is applied using a 1024 point FFT algorithm:

Task	Multiplications and Additions
input and format conversion	1 024
error linearization	1 024
FFT	40 960
inverse filter	4 096
FFT^{-1}	40 960
weighted update	8 192
output and format conversion	1 024
Sub-Total	97 280
contingency	52 720
TOTAL	150 000

If an update is to be performed for each 20 ms cycle, a floating point multiplication and accumulate (MAC) time of <130 ns is required. Digital signal processing (DSP) chips typically have a MAC time of 100 ns [9]. A 1024-point real FFT can be computed (in floating point arithmetic) within 2 ms using the latest DSP chips [10], which agrees with the estimate above. Use of such a DSP circuit would allow an update on every 20 ms cycle.

Using a 5 µs MAC-time for present-day 32-bit microprocessors (that are supported with a floating point co-processor), an update could be performed every 800 ms. Compared to a DSP circuit, a 'general purpose' processor is more capable of interfacing with a supervisory computer and handling multiple feedforward sequences. Multiple sequences would be stored by the processor, each for a given range of beam current. The expected beam current would be communicated to the processor from a supervisory computer. The appropriate sequence would then be used.

Processing requirements would be greatly reduced if the system inverse could be modelled using a finite impulse response filter or an infinite impulse response filter, provided less than 85 terms are required to define the filter. Because the tuner system is dominated by the solenoid and power supply responses, it is probable that a low-order filter would provide an adequate model. Investigation into this question on a similar system has shown the infinite impulse response filter approach to be feasible [11].

An important factor in the choice of a general purpose microprocessor or a DSP circuit is the TRIUMF in-house experience and capabilities. Use of a general purpose microprocessor that is already in use at TRIUMF can reduce development and maintenance times. Operational factors must also be considered. The added complication of a DSP chip may not carry any advantage if the beam current and acceleration cycle are sufficiently constant that rapid update of the feedforward sequence is not required.

Analog to digital and digital to analog converter resolution must be at least 14 bits to control to within 1 kHz over the 15 MHz range. If a 1024-point sequence is used, conversion times must be less than 19 μs.

Example components are:

summing junctions and gain	National LM6365 amplifier and LM6321 buffer. The amplifier has a gain-bandwidth product of 400 MHz and a slew rate of 180 V/μs. The buffer is capable of driving 50 Ω with a bandwidth of 30 MHz and a slew rate of 555 V/μs,
analog multiplier	AD539 (60 MHz signal bandwidth in multiplier configuration),
analog to digital converter	Motorola DSP56ADC16, 16 bit, 10 μs conversion time,
digital to analog converter	Analog Devices ADC 1146, 18 bit, 6 μs conversion time,
processor	Motorola 68030 with 68882 floating point co-processor, or: ADSP-2111, MC-DSP96002, or TI320C40 for the DSP option.

7.0 REFERENCES

[1] J. Elliott et al., "Kaon Factory Engineering Design and Impact Study, Report of the Steering Committee", TRIUMF, Vancouver, 1990 February.

[2] "Kaon Factory Study, Accelerator Design Report", TRIUMF, Vancouver, 1990.

[3] MATH/LIBRARY, IMSL, Houston, Texas, 1987, Version 1.0, pp. 633-639.

[4] R.L. Poirier et al., "A Perpendicular AC Biased Ferrite Tuned Cavity for the TRIUMF Kaon Factory Booster", conf. proceedings of EPAC, Nice, France, 1990 June, to be published.

[5] S. Koscielniak, "RF Noise Tolerances for the Kaon Factory", Design Note TRI-DN-89-K68, TRIUMF, Vancouver, 1990 September.

[6] L.K. Mestha, "Digital Feedback Control for Radial Beam Position", Rutherford Appleton Laboratories, RAL-89-091, September 1989.

[7] D. Boussard, "Variable Phase Shifter for the Fast RF Feedback in the Booster", TRIUMF Design Note TRI-DN-89-K82, 1989 October.

[8] T. Enegren, personal communications, TRIUMF, 1990 April.

[9] E.A. Lee, "Programmable DSP Architectures: Part II", IEEE ASSP Magazine, Vol. 6, no. 1, pp. 4-14, 1989 January.

[10] A. Bindra, "Trading Off DSP Specifications Per Application", Electronic Engineering TIMES, Special Issue: Microprocessor Design Guide, 1990, pp. 70 -71.

[11] L.K. Mestha, "The Applications of System Identification Techniques to an R.F. Cavity Tuning Loop", Rutherford Appleton Laboratories, RAL-89-101, September 1989.

APPENDIX A: ALC NORMALIZATION

It is shown below that use of the resonance controller dual channel ALC, in conjunction with a mixer (as shown in Figure 3-1), will produce a signal proportional to the error in tuning frequency.

Assumptions

1) The fast-feedback loop provides complete compensation; therefore, $\theta_v = 0$, and there is no error in $|v|$.

2) Cavity Q is sufficient that the following approximations are valid:

$$\tan \psi = \frac{2Q(f_0 - f)}{f_0} \qquad \text{(A-1)}$$

$$\frac{C(j\omega)}{C(j\omega_0)} = \cos \psi \angle \psi \qquad \text{(A-2)}$$

where, $C(j\omega)$ is the cavity shunt impedance at frequency ω.

Analysis

Let i_0 be the drive current required to produce v in the absence of beam, with no tuning error. The output of the mixer, e_r, will then be:

$$e_r = \frac{|i_p|}{|i_0|} * \sin \theta_p \qquad \text{(A-3)}$$

Since it is assumed that there is no error in **v**,

$$\frac{\mathbf{i}_t}{|\mathbf{i}_o|} * \cos\psi * 1\angle\psi = 1\angle 0 \qquad \text{(A-4)}$$

Using $\mathbf{i}_t = \mathbf{i}_g + \mathbf{i}_b$,

$$\frac{\mathbf{i}_p}{|\mathbf{i}_o|} = \frac{1\angle -\psi}{\cos\psi} - \frac{\mathbf{i}_b}{|\mathbf{i}_o|} \qquad \text{(A-5)}$$

Rewriting in rectangular coordinates:

$$\frac{\mathbf{i}_p}{|\mathbf{i}_o|} = 1 + Y\sin\theta_s + j(Y\cos\theta_s - \tan\psi) \qquad \text{(A-6)}$$

Using A-1 in A-6, A-3 can be rewritten as:

$$e_r = |1 + Y\sin\theta_s + j(Y\cos\theta_s - \tan\psi)| * \frac{\left(Y\cos\theta_s - \frac{2Q(f_0 - f)}{f_0}\right)}{|1 + Y\sin\theta_s + j(Y\cos\theta_s - \tan\psi)|} \qquad \text{(A-7)}$$

$$= Y\cos\theta_s - \frac{2Q(f_0 - f)}{f_0}$$

Therefore, e_r is linear with tuning frequency error.

If assumption 1 fails due to excessive tuning error and/or saturation of the final amplifier, the gain of the ALC – mixer circuit would increase provided the ALC were not at its limit.

APPENDIX B: TRACKING ERROR TO BANDWIDTH CONVERSION

To estimate the feedback phase control bandwidth and to estimate the tuner power supply bandwidth, a relationship between tracking error and bandwidth is found. It is assumed that the bandwidth is dominated by a single pole at ω_p and that the input is a simple 50 Hz triangular waveform. Using Laplace transform notation (with 's' as the Laplace variable), the system impulse response is:

$$C(s) = \frac{\omega_p}{s + \omega_p} \qquad \text{(B-1)}$$

The transform of a 10 ms unit ramp is:

$$R(s) = \frac{100}{s^2} \qquad \text{(B-2)}$$

Therefore, the system response to the ramp would be:

$$Y(s) = \left(\frac{100}{s^2}\right) * \left(\frac{\omega_p}{s + \omega_p}\right)$$

$$= 100\left[\frac{1}{s^2} + \frac{-1}{\omega_p s} + \frac{\omega_p^{-1}}{s + \omega_p}\right] \qquad \text{(B-3)}$$

Taking the difference between R(s) and Y(s) to give the error, E(s), it follows that:

$$e(t) = \left(\frac{100}{\omega_p}\right) * \left(1 - e^{-\omega_p t}\right) \qquad \text{(B-4)}$$

For $t < 10$ ms, e(t) is maximum at $t = 10^{-2}$. For the tuner power supply, $e(t)_{max}$ is specified as 0.125%; therefore, $\omega_p \geq 8*10^4$ radians/s (12.7 kHz). Similarly, for the feedback phase control electronics, for a specified maximum e(t) of $6.7*10^{-3}$, ω_p must be ≥ 15 k radians/s (2.4 kHz).

ISSN 0067-0367

To identify individual documents in the series we have assigned an AECL- number to each.

Please refer to the AECL- number when requesting additional copies of this document

from

Scientific Document Distribution Office
Atomic Energy of Canada Limited
Chalk River, Ontario, Canada
K0J 1J0

Price: A

ISSN 0067-0367

Pour identifier les rapports individuels faisant partie de cette série nous avons assigné un numéro AECL- à chacun.

Veuillez faire mention du numéro AECL- si vous demandez d'autres exemplaires de ce rapport

au

Service de Distribution des Documents Officiels
Énergie atomique du Canada limitée
Chalk River, Ontario, Canada
K0J 1J0

Prix: A

3206-90